Multi-band photometric stereo using random sampling of channels and pixels

Daisuke Miyazaki[0000−0002−7312−0543] and Koumei Hamaen[1]

Hiroshima City University, Hiroshima 731-3194, Japan
miyazaki@hiroshima-cu.ac.jp
http://www.info.hiroshima-cu.ac.jp/˜miyazaki/

Abstract. One of the main problems faced by the photometric stereo method is that several measurements are required, as this method needs illumination from light sources from different directions. A solution to this problem is the color photometric stereo method, which conducts one-shot measurements by simultaneously illuminating lights of different wavelengths. However, the classic color photometric stereo method only allows measurements of white objects, while a surface-normal estimation of a multicolored object using this method is theoretically impossible. This paper estimates the surface normal of a multi-colored object under multi-spectral lighting. This is a difficult problem since the albedo is different for each pixel and each channel. We solve this problem by sampling some pixels randomly. If we randomly sample neighboring pixels, the probability of picking the same albedo pixels may be high. Therefore, if the sampled pixels all have the same albedo, we can determine the surface normal uniquely. To demonstrate the effectiveness of this study, a measurement device with seven colors is used.

Keywords: photometric stereo · color photometric stereo · multispectral camera · multiple albedo · random sampling

1 Introduction

The color photometric stereo method involves placing light sources of red, green, and blue colors in three different directions, which simultaneously illuminate the target object. This paper proposes a technique that employs a random sampling approach so that it can be applied to colored objects, which is impossible for conventional color photometric stereo.

The photometric stereo method [23, 26] requires capturing three pictures with different light source directions. Therefore, it is impossible to measure a dynamic object. This problem can be resolved using the color photometric stereo method [1–8, 11–16, 19, 21, 22, 24, 25, 27]. In this method, lights are simultaneously illuminated from red, green, and blue light sources, and one picture photographed with an RGB color camera is captured. The principle problem of the color photometric stereo method is the fact that it can only be used with white objects.

---

[1] Current address: Fujitsu Frontech Ltd.

Recently, some amount of techniques have been proposed to apply the color photometric stereo method to multicolored objects [1, 3, 8–10, 13, 14, 17, 22].

In this paper, we solve the problem by sampling some pixels randomly. If we randomly sample neighboring pixels, the probability of picking the same albedo pixels may be high. Therefore, if the sampled pixels all have the same albedo, we can determine the surface normal uniquely. We try the sampling process multiple times with different combinations, and we choose the representative surface normal among the multiple trials.

Unlike existing methods, we neither apply optical flow algorithm [9, 14, 22], nor apply region segmentation algorithm [8]. Unlike existing methods, our method is not limited to achromatic objects [10], and is not oversmoothed by median filtering [17]. Unlike existing methods, we neither need reflectance database [8], nor need shape from other sensors [1].

2   Multispectral color photometric stereo method

2.1   Image formulation

Suppose that we lit a single parallel light source (infinite-far point light source) whose spectral distribution is represented as delta function, the pixel brightness I_c of channel c can be represented as follows using the Lambertian reflection model.

$$I_c = A_c \max(\mathbf{n} \cdot \mathbf{l}_c, 0) \quad . \tag{1}$$

Here, $\mathbf{n}$ is a normal vector and $\mathbf{l}_c$ is the light source direction vector of channel c. Hereinafter, we call A_c albedo. Note that the camera sensitivity and light source brightness are included in A_c.

As shown in Fig. 1, this study conducts a photoshoot of a multicolored object using seven channels. Following Eq. (1), the brightness is obtained from this photoshoot as follows.

$$
\begin{aligned}
I_0 &= A_0 \max(\mathbf{n} \cdot \mathbf{l}_0, 0) \quad , \\
I_1 &= A_1 \max(\mathbf{n} \cdot \mathbf{l}_1, 0) \quad , \\
&\vdots \\
I_6 &= A_6 \max(\mathbf{n} \cdot \mathbf{l}_6, 0) \quad .
\end{aligned}
\tag{2}
$$

The surface normal $\mathbf{n}$ is a 3D vector; however, the degree-of-freedom is two because it is constrained to be a unit vector (such constraint reduces one degree-of-freedom). Albedo A_c is represented by seven parameters. There are seven equations, as shown in Eq. (2), and nine unknown parameters (A_0, A_1, ..., A_6, n_x, n_y, n_z, s.t., $n_x^2 + n_y^2 + n_z^2 = 1$, namely seven for albedo and two for surface normal). Therefore, color photometric stereo, without any assumption or constraint, is an ill-posed problem.

The most commonly used assumption is to limit the color of the target objects to white ($A_0 = A_1 = \ldots = A_6$). The color photometric stereo for white objects,
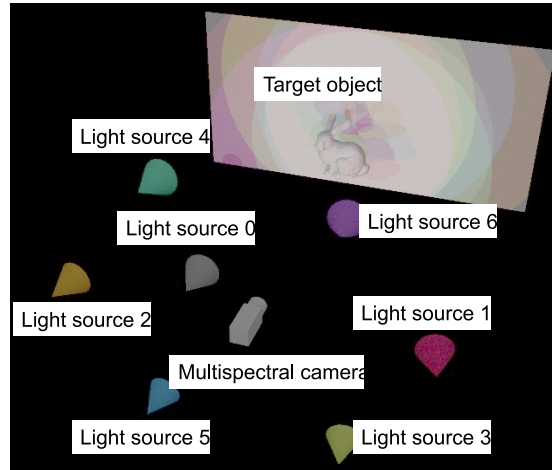
Fig. 1. Conceptual explanation of multispectral color photometric stereo. Target object is illuminated by multiple light sources whose wavelengths are different. One image is taken using multispectral camera.

or in other words, the conventional photometric stereo can directly solve the surface normal.

However, this paper analyzes the methods with multi-colored objects. Therefore, we randomly sample some pixels that can be assumed to be the same albedo. The unknown normal parameters (n_x, n_y, n_z) increase if we use multiple pixels. The unknown albedo parameters $(A_0, A_1, \ldots, A_6)$ also increase if the chosen pixels have a different albedo, while they do not increase if the chosen pixels have the same albedo because $A_0, A_1, \ldots, A_6$ are the same for all chosen pixels. In the latter case, the number of equations is more than the number of unknowns, thus, the problem becomes solvable. If the chosen pixels have the same albedo, the correct surface normal can be estimated. However, the surface normal cannot be estimated correctly if the chosen pixels have different albedo. To overcome this problem (Fig. 1), Section 2.2 shows our method which can be applied to the object surface of non-uniform albedo.

### 2.2   Multiple albedo with 4 channels and 8 pixels

Our method chooses some channels and some pixels randomly, and estimates the surface normal from chosen data. The problem is that the albedo of chosen pixels might be different from that of the pixel of interest (Fig. 2). Fig. 3 is the example of randomly chosen pixels.

Another problem is that the estimation will fail if we choose the channels that contain shadow or specular reflection (Fig. 4).

Chosen pixels should be the same albedo, thus, we choose the pixels which are spatially close to the pixel of interest. Suppose that we choose 8 pixels (Fig. 5).
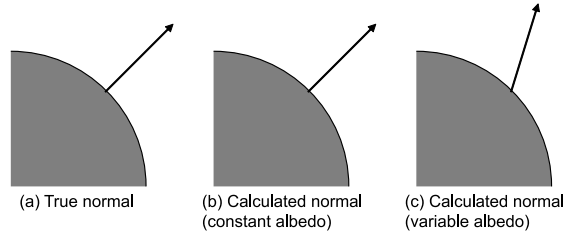
**Fig. 2.** Example of estimated surface normal.
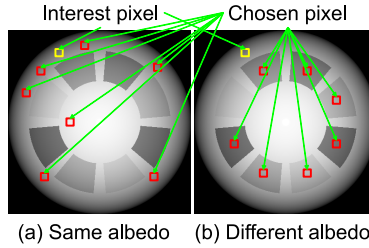
Fig. 3. Chosen pixels: (a) Pixels chosen from same albedo and (b) pixels chosen from different albedo.

First, we denote the pixel of interest as P_0. Next, we choose 1 pixel P_1 from 3×3 pixels surrounding the pixel of interest. Similarly, we choose P_2 from 7×7 area. And, we choose P_3, P_4, P_5, P_6, and P_7 from 13×13, 21×21, 29×29, 41×41, and 55×55, respectively. As shown in Fig. 6, even if the interest pixel is at the boundary of multiple albedos, it is likely to choose the pixels with the same albedo. Usually, the object is painted with the same paint for a certain amount of region. Thus, it is statistically apparent that neighboring pixels have a high probability to be the same albedo.
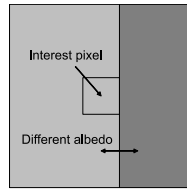
This paper uses 8 for the number of pixels to be chosen. The optimal number to be chosen depends on the surrounding pixels whether they have uniform albedo or they have various albedos. Therefore, we cannot determine a constant
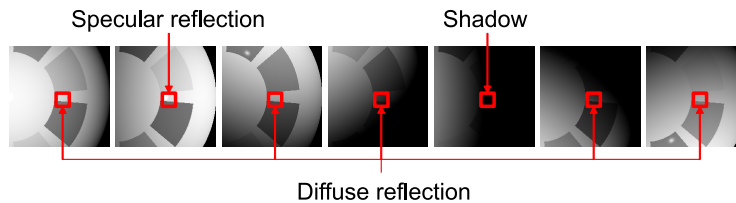
Fig. 4. Example of pixel brightness for each channel.
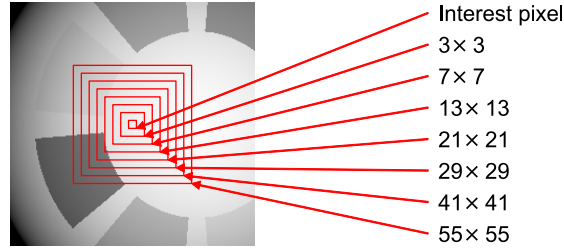
Fig. 5. Selecting area of pixels.

Fig. 6. Interest pixel at the boundary of multiple albedo.

number for chosing pixels that works for every pixel. As shown in the experiments (Section 3), we have empirically found that 8 is the best number for chosing pixels.

To avoid shadow, we choose the channels that have large brightness. We choose the channels randomly to avoid specular reflection. Suppose that we choose 4 channels from 7 channels. First, we sum up the brightness of the pixel of interest for each channel.

$$I_{sum} = I_{0,0} + I_{0,1} + \cdots + I_{0,6} \,. \tag{3}$$

We represent the probability P_c as Eq. (4), which is the brightness of each channel divided by the sum.

$$P_c = \frac{I_{0,c}}{I_{sum}} \,. \tag{4}$$

We choose the channel a using Eq. (5), where R is a random number from 0 to 1.

$$0 \le R < P_1 \ (a = 0) \,,$$
$$\sum_{i=0}^{a-1} P_i \le R < \sum_{i=0}^{a} P_i \ (\text{otherwise}) \,. \tag{5}$$

Let us denote the chosen channel a as C_0. We set the value I_{0,C_0} to be 0, recalculate Eq. (3) and Eq. (4), and we determine C_1 from Eq. (5). Similarly, we determine C_2 and C_3.

2.3   Computing albedo and surface normal

The cost function for 4 channels and 8 pixels is shown in Eq. (6).

$$\arg\min \sum_{a=0}^{7} \sum_{b=0}^{3}$$
$$(I_{P_a,C_b} - A_{C_b}(n_{P_a,x}l_{C_b,x} + n_{P_a,y}l_{C_b,y} + n_{P_a,z}l_{C_b,z}))^2. \tag{6}$$
$$\text{s.t.} \quad n_{P_a,x}^2 + n_{P_a,y}^2 + n_{P_a,z}^2 = 1 \quad (a = 0,1,\cdots,7).$$

Eq. (6) has 20 unknown parameters, which are the albedo $(A_{C_0}, A_{C_1}, A_{C_2}, A_{C_3})$ (4 parameters) and the normal $\mathbf{n}_p$ (2×8 parameters). Pixel brightness $I_{P,C}$ is the input, and the light source direction $\mathbf{l}_C$ is known. Therefore, Eq. (6) is solvable since the number of equations is 32 and the number of unknowns is 20. We minimize Eq. (6) using alternative minimization. We fix albedo and compute surface normal, next we fix surface normal and compute albedo, and we repeat this alternating minimization until convergence. This alternating minimization approach is proved to converge.

If we assume that the albedo A_C is known, we have a closed-form solution of Eq. (6), and we obtain the surface normal $\mathbf{n}$ as $\mathbf{n} = \mathbf{L}^{-1}\mathbf{s}$.

$$\mathbf{Ln} = \mathbf{s}, \tag{7}$$

$$\mathbf{L} = \begin{pmatrix} l_{C_0,x} & l_{C_0,y} & l_{C_0,z} & & \\ l_{C_1,x} & l_{C_1,y} & l_{C_1,z} & & \\ l_{C_2,x} & l_{C_2,y} & l_{C_2,z} & & \\ l_{C_3,x} & l_{C_3,y} & l_{C_3,z} & & \\ & & & l_{C_0,x} & \cdots \\ & & & \vdots & \ddots \end{pmatrix}, \mathbf{n} = \begin{pmatrix} n_{P_0,x} \\ n_{P_0,y} \\ n_{P_0,z} \\ n_{P_1,x} \\ \vdots \\ nP_7, z \end{pmatrix}, \mathbf{s} = \begin{pmatrix} \frac{I_{P_0,C_0}}{A_{C_0}} \\ \frac{I_{P_0,C_1}}{A_{C_1}} \\ \frac{I_{P_0,C_2}}{A_{C_2}} \\ \frac{I_{P_0,C_3}}{A_{C_3}} \\ \frac{I_{P_1,C_0}}{A_{C_0}} \\ \vdots \\ \frac{I_{P_7,C_3}}{A_{C_3}} \end{pmatrix}.$$

If we assume that the surface normal $n_{P_a,x}, n_{P_a,y}, n_{P_a,z}$ is known, we have a closed-form solution of Eq. (6), and we obtain the albedo as Eq. (8).

$$A_{C_b} = \text{median}(\frac{I_{P_0,C_b}}{n_{P_0,x}l_{C_b,x} + n_{P_0,y}l_{C_b,y} + n_{P_0,z}l_{C_b,z}},$$
$$\frac{I_{P_1,C_b}}{n_{P_1,x}l_{C_b,x} + n_{P_1,y}l_{C_b,y} + n_{P_1,z}l_{C_b,z}},$$
$$\cdots, \frac{I_{P_7,C_b}}{n_{P_7,x}l_{C_b,x} + n_{P_7,y}l_{C_b,y} + n_{P_7,z}l_{C_b,z}}). \tag{8}$$

If the surface normal $\tilde{n}_{P_a,x}, \tilde{n}_{P_a,y}, \tilde{n}_{P_a,z}$ is given, the closed-from solution $n_{P_a,x}, n_{P_a,y}, n_{P_a,z}$ of Eq. (9) will be Eq. (10).

$$\min\{(n_{P_a,x} - \tilde{n}_{P_a,x})^2 + (n_{P_a,y} - \tilde{n}_{P_a,y})^2 + (n_{P_a,z} - \tilde{n}_{P_a,z})^2\}, \tag{9}$$
$$\text{s.t.} \quad n_{P_a,x}^2 + n_{P_a,y}^2 + n_{P_a,z}^2 = 1.$$
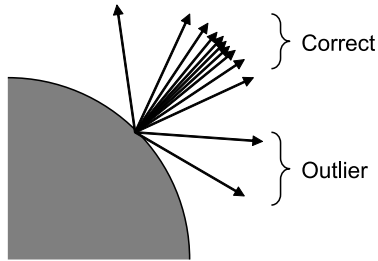
Fig. 7. Candidate surface normals.

$$(n_{P_a,x}, n_{P_a,y}, n_{P_a,z}) = \frac{\tilde{n}_{P_a,x}, \tilde{n}_{P_a,y}, \tilde{n}_{P_a,z}}{\sqrt{\tilde{n}_{P_a,x}^2 + \tilde{n}_{P_a,y}^2 + \tilde{n}_{P_a,y}^2}} . \tag{10}$$

As a result, if the initial values of $A_{C_0}, A_{C_1}, A_{C_2}, A_{C_3}$ are given, the albedo $A_{C_0}, A_{C_1}, A_{C_2}, A_{C_3}$ and the surface normal $n_{P_0,x}, n_{P_0,y}, \cdots, n_{P_7,z}$ are obtained by iteratively calculating Eq. (7), Eq. (8), and Eq. (10).

The chosen pixels and channels do not always contain the diffuse reflection with constant albedo. Therefore, we choose the set of channels and pixels 64 times. For each set of 64 sets, the candidates of surface normal can be obtained (Fig. 7). The surface normal $\mathbf{n}_m$ $(m = 1, \ldots, a)$ is calculated for each set when we make a numbers of sets with randomly chosen channels and pixels. Surface normal is calculated by Eq. (11).

$$\mathbf{n} = \text{median}(\mathbf{n}_m | m = 1, \ldots, a). \tag{11}$$

The pseudo-code of the algorithm is shown in Algorithm 1.

3   Experiment

Fig. 8 shows a diagram of the experiment.

The camera used for this experiment is an FD-1665 (FluxData, Inc., USA) multi-spectral camera. Figure 9 shows the spectral sensitivity of the camera. As shown in Fig. 9, channel crosstalk occurred among all camera channels. Therefore, the method shown in Miyazaki et al. [17] is used to remove the channel crosstalk in the photographed input image.

Table 1 shows the full width at half maximum (FWHM) for each light source used in this experiment. Although our algorithm can be applied to natural illumination, most natural scene does not contain the variety of lights with different wavelengths. Our method cannot be applied to natural illumination due to the hardware problem, and thus, we used the system shown in Fig. 8.

Fig. 10 (a) shows the albedo of synthetic object, and Fig. 10 (b) shows its input image. Fig. 11 (a)–(d) show the result of the surface normal when 3 channels 4 pixels, 4 channels 8 pixels, 4 channels 16 pixels, and 7 channels 16 pixels


Algorithm 1 Proposed algorithm

1: **for** object region **do**
2:     List $\Leftarrow$ empty
3:     **for** 64 sets **do**
4:       Choose 4 channels
5:       Choose 8 pixels
6:       $A_{C_0}, A_{C_1}, A_{C_2}, A_{C_3} \Leftarrow$ initial value
7:       $\mathbf{L} \Leftarrow$ light source direction
8:       **for** Until convergence **do**
9:         **for** $a = 0, 1, \cdots, 7$ **do**
10:           **for** $b = 0, 1, 2, 3$ **do**
11:             $\mathbf{s} \Leftarrow \frac{I_{P_a, C_b}}{A_{C_b}}$
12:           **end for**
13:         **end for**
14:         $\mathbf{n} \Leftarrow \mathbf{L}^+ \mathbf{s}$
15:         **for** $p = 0, 1, \cdots, 7$ **do**
16:           $\mathbf{n}_{P_a} \Leftarrow \frac{\mathbf{n}_{P_a}}{\|\mathbf{n}_{P_a}\|}$
17:         **end for**
18:         **for** $c = 0, 1, 2, 3$ **do**
19:           $A_{C_b} \Leftarrow \text{median}(\frac{I_{P_0, C_b}}{\mathbf{n}_{P_0} \mathbf{l}_{C_b}}, \frac{I_{P_1, C_b}}{\mathbf{n}_{P_1} \mathbf{l}_{C_b}}, \cdots, \frac{I_{P_7, C_b}}{\mathbf{n}_{P_7} \mathbf{l}_{C_b}})$
20:         **end for**
21:         $List \Leftarrow List + \mathbf{n}_{P_0}$
22:       **end for**
23:     **end for**
24:     Normal $\Leftarrow \text{median}(List)$
25: **end for**
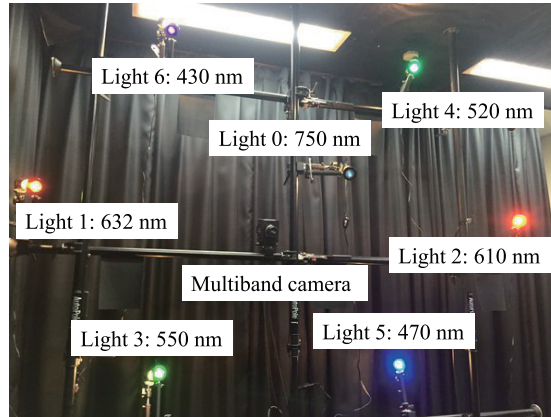
Fig. 8. Experimental setup with 7 light sources with different wavelengths and a single 7-band multispectral camera.
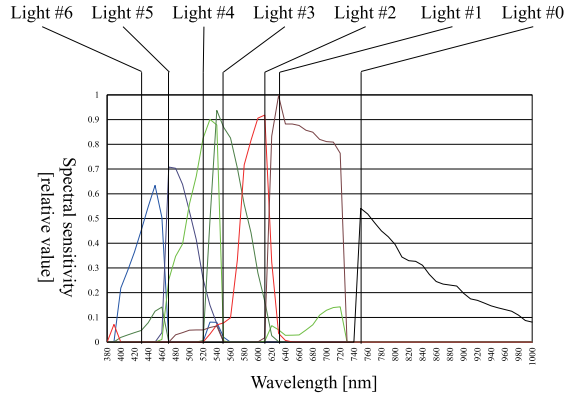
Fig. 9. Spectral sensitivity of multispectral camera and peak wavelength of each light sources.

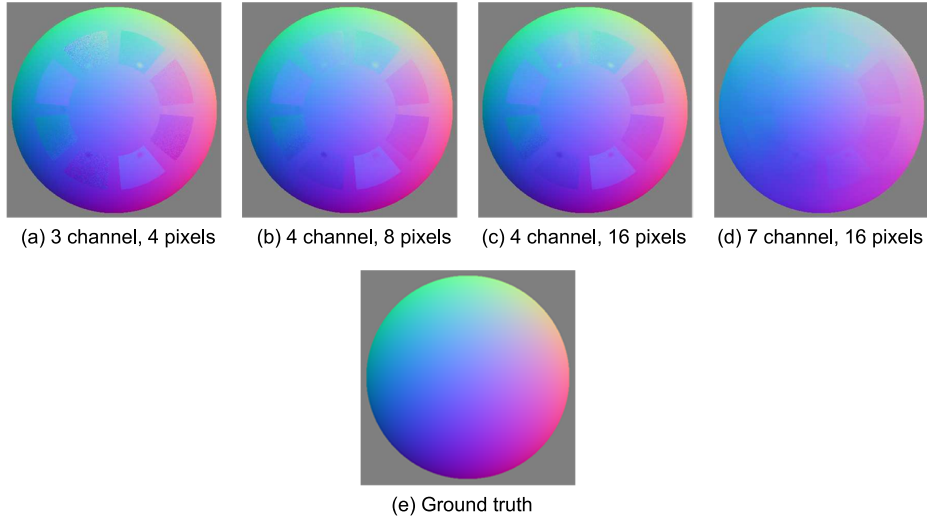**Table 1.** Peak wavelength and FWHM for each light source.

Light	0	1	2	3	4	5	6
Peak	750nm	632nm	610nm	550nm	520nm	470nm	430nm
FWHM	10nm	10nm	10nm	10nm	10nm	10nm	10nm

are chosen, respectively. Fig. 11 (e) is the ground truth where R, G, and B colors represent x, y, and z axes, respectively. The average error depending on the number of channels and pixels is shown in Fig. 12. Fig. 13 shows the reconstructed shape of Fig. 11 (b).

Fig. 14 shows the comparison between our method and other methods. Here, the conventional photometric stereo (Fig. 14 (a)) means the color photometric stereo where the object is white. Average errors of the conventional photometric stereo (Fig. 14 (a)) and the proposed method (Fig. 14 (c)) were both 0.064 [rad], and that of the method by Guo et al. [10] (Fig. 14 (b)) was 0.213 [rad]. Compared
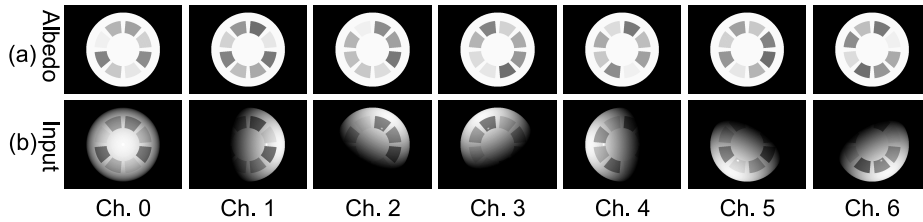
Fig. 10. Virtual sphere for each channel: (a) The albedo and (b) input image.

(a) 3 channel, 4 pixels   (b) 4 channel, 8 pixels   (c) 4 channel, 16 pixels   (d) 7 channel, 16 pixels

(e) Ground truth

Fig. 11. Estimated normal of virtual sphere: (a) 3 channels 4 pixels, (b) 4 channels 8 pixels, (c) 4 channels 16 pixels, (d) 7 channels 16 pixels, and (e) ground truth.


(a) 8 pixels   (b) 4 channels
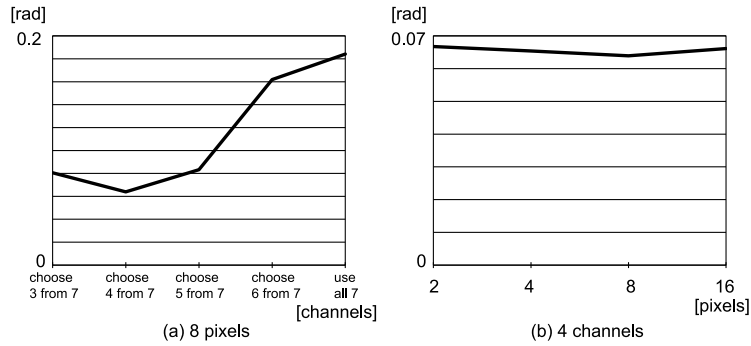
Fig. 12. The average error for different number of channels and pixels: (a) Error of 8 pixels and (b) error of 4 channels.

to the color photometric stereo for white objects (Fig. 14 (a)), where the shadow boundary is apparent, the proposed method (Fig. 14 (c)) produces the result which is not affected by outliers such as shadows.

Fig. 11 (a) has more noise than Fig. 11 (b) since the number of selected pixels is not enough. The color of Fig. 11 (d) is vague compared to Fig. 11 (c), which means that the estimated shape of Fig. 11 (d) is flat. The reason that Fig. 11 (c) is better than Fig. 11 (d) is that the channels including shadow are chosen. Therefore, also considering Fig. 12, it is adequate to choose 4 channels and 8 pixels.
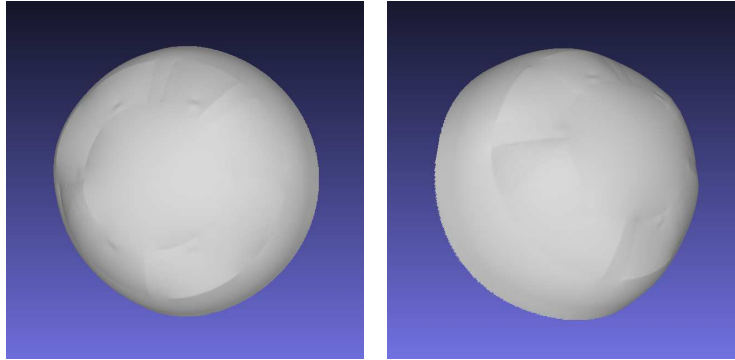
Fig. 13. Estimated shape of virtual sphere.

(a) Photometric stereo (b) Previous method (c) Proposed method
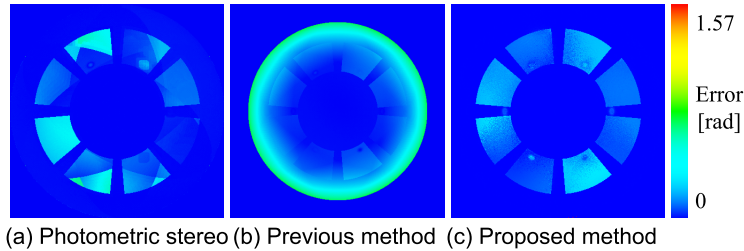
Fig. 14. Error map between estimated normal and true normal: (a) Error of conventional photometric stereo, (b) error of existing method, and (c) error of proposed method.
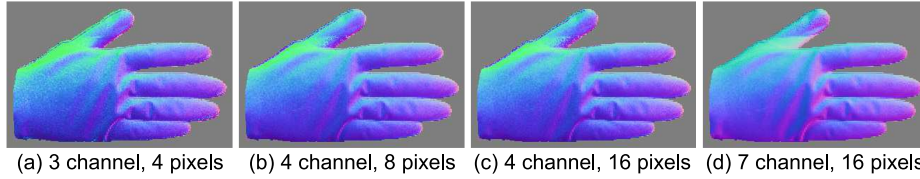
The input image of a glove is shown in Fig. 15. Fig. 16 (a)–(d) show the result of 3 channels 4 pixels, 4 channels 8 pixels, 4 channels 16 pixels, and 7 channels 16 pixels, respectively. Fig. 17 is the shape integrated from the estimated surface normal. Fig. 17 empirically proved that the dynamically deforming object such as hand can be estimated by using the proposed method. The glove can change its shape such as wrinckles depending on the motion of a human hand. If we take multiple photos of the target glove, the glove cannot be stably fixed. On the other hand, our system can take one photo, thus, we can estimate the moving objects.

An object of a doll is shown in Fig. 18. The input image of a doll is shown in Fig. 19. Fig. 20 (a)–(d) show the result of 3 channels 4 pixels, 4 channels 8 pixels, 4 channels 16 pixels, and 7 channels 16 pixels, respectively. Fig. 21 is the shape integrated from the surface normal shown in Fig. 20 (b). Fig. 20 (b) empirically proved that the proposed method successfully estimated the surface normal even if the object has multiple albedos.

One failure part of our method can be the red basket placed in the lower part of the doll. In addition, the noise contained in the result is also the problem

Ch. 0   Ch. 1   Ch. 2   Ch. 3   Ch. 4   Ch. 5   Ch. 6

Fig. 15. Hand of each channel.

(a) 3 channel, 4 pixels   (b) 4 channel, 8 pixels   (c) 4 channel, 16 pixels   (d) 7 channel, 16 pixels
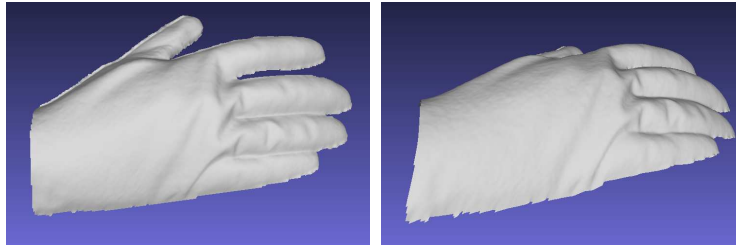
Fig. 16. Estimated normal of hand: (a) 3 channels 4 pixels, (b) 4 channels 8 pixels, (c) 4 channels 16 pixels, (d) 7 channels 16 pixels.

of our method. Median filtering can solve the problem, but the result will be oversmoothed. To overcome the problem fundamentally, our future work will be to increase the number of light sources (channels).

4   Conclusion

In this study, surface normal estimation of multicolored objects was conducted by the multi-spectral color photometric stereo method. We estimated the surface normal using randomly chosen channels and pixels.

Our approach which randomly selects the pixels and the channels is statistically convincing, however, it is not assured to choose the best combination. An alternative approach to random selection is to apply region segmentation a priori. However, we cannot use the color information for region segmentation because each light source has different colors, and thus, we cannot distinguish

**Fig. 17.** Estimated shape of hand.

Fig. 18. Target object.

| Ch. 0 | Ch. 1 | Ch. 2 | Ch. 3 | Ch. 4 | Ch. 5 | Ch. 6 |
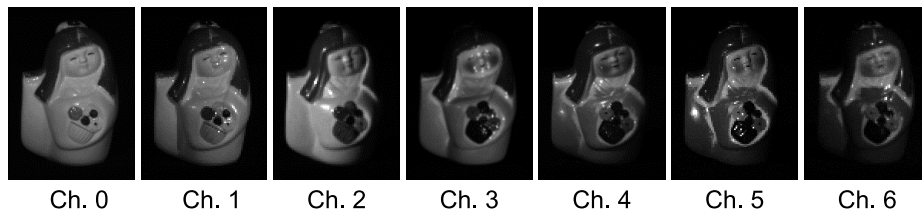
Fig. 19. Doll of each channel.

between the object color and the light color. This is why we did not apply region segmentation. However, if the neighboring pixels have the same albedo and similar normal, we can apply the region-growing method to segment the image since the neighboring pixels have similar data. One of our plans is to apply a region-growing method to improve the performance of our method.

(a) 3 ch., 4 pix.   (b) 4 ch., 8 pix.   (c) 4 ch., 16 pix.   (d) 7 ch., 16 pix.
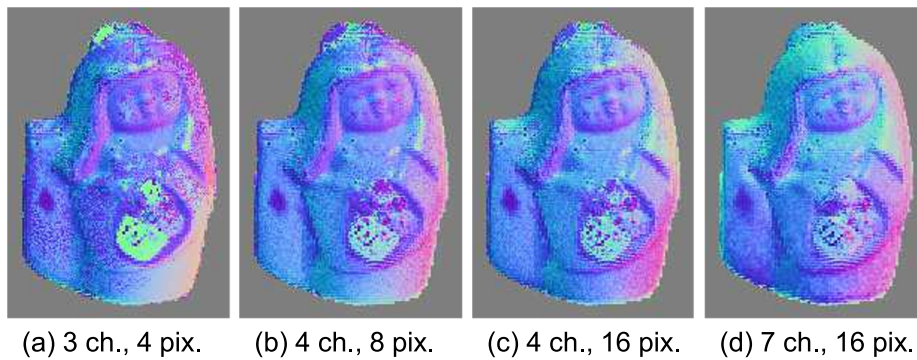
Fig. 20. Estimated normal of doll: (a) 3 channels 4 pixels, (b) 4 channels 8 pixels, (c) 4 channels 16 pixels, (d) 7 channels 16 pixels.
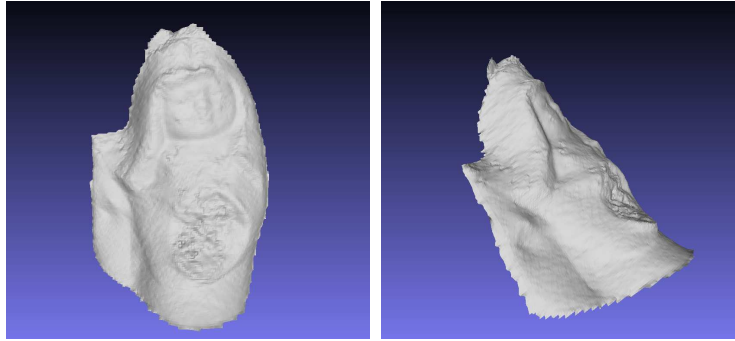
Fig. 21. Estimated shape of doll.

Ideally, the specular reflection only appears in one channel, and thus our approach is reliable. However, actual specular reflection does not have a spiky shape but is broadened widely. Therefore, multiple channels may contain specular reflection which violates our assumption. To overcome this problem, we are planning to increase the number of channels (*i.e.*, the number of light sources) so that the number of diffuse channels becomes larger than the number of specular channels.

Considering that the color photometric stereo is an ill-posed problem (Section 2.1), our method is enough good to solve this difficult problem. However, we still think that our method is not outputting a satisfactory result. Due to the difficult problem tackling, drastic update is needed, and the fundamental improvement of this work will be our future goal.

References

1. R. Anderson, B. Stenger, and R. Cipolla, "Color photometric stereo for multicolored surfaces," In *International Conference on Computer Vision*, pp. 2182-2189, 2011.
2. G. J. Brostow, B. Stenger, G. Vogiatzis, C. Hernández, and R. Cipolla, "Video normals from colored lights," *IEEE Transactions on Pattern Analysis & Machine Intelligence*, vol. 33, no. 10, pp. 2104–2114, 2011.
3. A. Chakrabarti and K. Sunkavalli, "Single-image RGB photometric stereo with spatially-varying albedo," In *International Conference on 3D Vision*, pp. 258–266, 2016.
4. M. S. Drew, "Reduction of rank-reduced orientation-from-color problem with many unknown lights to two-image known-illuminant photometric stereo," In *Proceedings of International Symposium on Computer Vision*, pp. 419–424, 1995.
5. M. S. Drew, "Direct solution of orientation-from-color problem using a modification of Pentland's light source direction estimator," *Computer Vision and Image Understanding*, vol. 64, no. 2, pp. 286–299, 1996.

6. M. S. Drew and M. H. Brill, "Color from shape from color: a simple formalism with known light sources," *Journal of the Optical Society of America A*, vol. 17, no. 8, pp. 1371–1381, 2000.

7. M. Drew and L. Kontsevich, "Closed-form attitude determination under spectrally varying illumination," In *IEEE Conference on Computer Vision and Pattern Recognition*, pp. 985–990, 1994.

8. G. Fyffe, X. Yu, and P. Debevec, "Single-shot photometric stereo by spectral multiplexing," *IEEE International Conference on Computational Photography*, pp. 1–6, 2011.

9. P. F. U. Gotardo, T. Simon, Y. Sheikh, and I. Mathews, "Photogeometric scene flow for high-detail dynamic 3D reconstruction," In *IEEE International Conference on Computer Vision*, pp. 846–854, 2015.

10. H. Guo, F. Okura, B. Shi, T. Funatomi, Y. Mukaigawa, and Y. Matsushita, "Multispectral photometric stereo for spatially-varying spectral reflectances: A well posed problem?," In *IEEE/CVF Conference on Computer Vision and Pattern Recognition*, pp. 963–971, 2021.

11. C. Hernandez, G. Vogiatzis, G. J. Brostow, B. Stenger, and R. Cipolla, "Non-rigid photometric stereo with colored lights," In *IEEE International Conference on Computer Vision*, pp. 8, 2007.

12. C. Hernández, G. Vogiatzis, and R. Cipolla, "Shadows in three-source photometric stereo," In *ECCV 2008*, pp. 290–303, 2008.

13. H. Jiao, Y. Luo, N. Wang, L. Qi, J. Dong, and H. Lei, "Underwater multi-spectral photometric stereo reconstruction from a single RGBD image," In *Asia-Pacific Signal and Information Processing Association Annual Summit and Conference*, pp. 1–4, 2016.

14. H. Kim, B. Wilburn, and M. Ben-Ezra, "Photometric stereo for dynamic surface orientations," In *European Conference on Computer Vision*, LNCS 6311, pp. 59–72, 2010.

15. L. Kontsevich, A. Petrov, and I. Vergelskaya, "Reconstruction of shape from shading in color images," *Journal of Optical Society of America A*, vol. 11, pp. 1047–1052, 1994.

16. A. Landstrom, M. J. Thurley, and H. Jonsson, "Sub-millimeter crack detection in casted steel using color photometric stereo," In *International Conference on Digital Image Computing: Techniques and Applications*, pp. 1–7, 2013.

17. D. Miyazaki, Y. Onishi, and S. Hiura, "Color photometric stereo using multi-band camera constrained by median filter and occluding boundary," *Journal of Imaging*, vol. 5, no. 7, article no. 64, 29 pages, 2019.

18. F. E. Nicodemus, J. C. Richmond, J. J. Hsia, I. W. Ginsberg, and T. Limperis, "Geometrical considerations and nomenclature of reflectance," In *Radiometry*; L. B. Wolff, S. A. Shafer, and G. Healey; Jones and Bartlett Publishers, Inc.: USA, 1992; pp.940–145.

19. A. P. Petrov and L. L. Kontsevich, "Properties of color images of surfaces under multiple illuminants," *J. Opt. Soc. Am. A*, vol. 11, no. 10, pp. 2745–2749, 1994.

20. Y. Quéau, R. Mecca, J.-D. Durou, "Unbiased photometric stereo for colored surfaces: A variational approach," In *IEEE Conference on Computer Vision and Pattern Recognition*, pp. 4359–4368, 2016.

21. S. Rahman, A. Lam, I. Sato, and A. Robles-Kelly, "Color photometric stereo using a rainbow light for non-Lambertian multicolored surfaces," In *Asian Conference on Computer Vision*, pp. 335–350, 2015.

22. N. Roubtsova and J. Y. Guillemaut, "Colour Helmholtz stereopsis for reconstruction of complex dynamic scenes," In *International Conference on 3D Vision*, pp. 251–258, 2014.

23. W. M. Silver, "Determining shape and reflectance using multiple images," *Master's thesis*, Massachusetts Institute of Technology, 1980.

24. G. Vogiatzis and C. Hernández, "Practical 3d reconstruction based on photometric stereo," pp. 313–345. In: R. Cipolla, S. Battiato, and G. M. Farinella, "Computer Vision: Detection, Recognition and Reconstruction," *Springer Berlin Heidelberg*, Berlin, Heidelberg, 2010.

25. G. Vogiatzis and C. Hernandez, "Self-calibrated, multi-spectral photometric stereo for 3D face capture," *Int. J. Comput. Vis.*, vol. 97, pp. 91–103, 2012.

26. R. J. Woodham, "Photometric method for determining surface orientation from multiple images," *Optical Engineering*, vol. 19, no. 1, pp. 139–144, 1980.

27. R. J. Woodham, "Gradient and curvature from photometric stereo including local confidence estimation," *Journal of the Optical Society of America*, vol. 11, pp. 3050–3068, 1994.